ELSEVIER

Journal of Fluids and Structures 26 (2010) 658–674

JOURNAL OF FLUIDS AND STRUCTURES

www.elsevier.com/locate/jfs

Experimental study of wall pressure fluctuations in rigid and elastic pipes behind an axisymmetric narrowing

A.O. Borisyuk*

Institute of Hydromechanics, Zhelyabova Str. 8/4, 03680 Kyiv 180 MSP, Ukraine

Received 15 February 2007; accepted 17 February 2010
Available online 9 April 2010

Abstract

Wall pressure fluctuations, p_t, in rigid and elastic pipes behind a local axisymmetric narrowing are studied. A sharp increase in their rms level in a finite region immediately downstream of the narrowing, leading up to a pronounced maximum upstream of the point of jet reattachment, is found. Approximate estimates both for the distance from the narrowing to the point of maximum rms pressure and for the rms magnitude at this point are obtained. Inspection of the wall pressure power spectrum, P, reveals the presence of low-frequency maxima. The maxima are found to be associated with the large-scale eddies in the regions of separated and reattached flow, and their frequencies are close to the characteristic frequencies of the eddies' formation. These maxima are the main distinguishing features of the spectrum under investigation compared to the power spectrum of the wall pressure fluctuations in a fully-developed turbulent flow in a pipe without narrowing. A comparative analysis of the data for rigid and elastic pipes shows that changes in the pipe wall bending stiffness cause alterations in the flow structure near the wall and the corresponding redistribution of flow energy among the vortices. This results in an increase in the wall pressure amplitude and the low-frequency level of the wall pressure power spectrum, as well as the appearance of new frequency components in this domain.

Keywords: Pipe; Narrowing; Disturbed flow; Wall pressure fluctuations

1. Introduction

Local stenotic narrowings of blood vessels are often the reason for serious circulatory disorders. They can result in ischemia of body organs and tissues, high blood pressure, changes in the structure and properties of the vessel wall material, production of blood clots, etc. (Berger and Jou, 2000; Mirolyubov, 1983; Young, 1979). As the relevant clinical studies show, the stronger the stenosis the more severe is the disease caused by it. Therefore, the detection of a stenosis at an early stage in its development is an important practical problem.

The most popular method for obtaining information about a stenosis is arteriography. It is based on the injection of a Roentgen-contrast fluid into the artery via a catheter, the formation of an X-ray-image of the region of interest, and subsequent study of that image in order to determine the degree of vessel obstruction. However, this technique is

*Tel.: +38 44 450 5110; fax: +38 44 455 6432.
E-mail address: aobor@mail.ru

0889-9746/$ - see front matter © 2010 Elsevier Ltd. All rights reserved.
doi:10.1016/j.jfluidstructs.2010.03.005

Nomenclature

D	pipe diameter
$D_v^{(e)}$	bending stiffness coefficient of an elastic pipe
$D_v^{(r)}$	bending stiffness coefficient of a rigid pipe
d	narrowing diameter
f	frequency
$f_{ch}^{(i)}$	characteristic frequencies of vortex formation ($i = 1, \ldots, 3$)
H	difference between the levels of water in upper and lower reservoirs
h	narrowing wall thickness
$L_{\max}$	distance from narrowing to the point of maximum pressure p_{rms}
$L_{\max}^{(e)}$	distance from narrowing to the point of maximum pressure $p_{\mathrm{rms}}^{(e)}$
$L_{\max}^{(r)}$	distance from narrowing to the point of maximum pressure $p_{\mathrm{rms}}^{(r)}$
l	narrowing length
P	power spectrum of the wall pressure fluctuations behind narrowing
P_e	power spectrum of the wall pressure fluctuations behind narrowing in an elastic pipe
P_r	power spectrum of the wall pressure fluctuations behind narrowing in a rigid pipe
P_0	power spectrum of the wall pressure fluctuations in fully-developed turbulent flow in rigid pipe without narrowing
p_{rms}	root-mean-square wall pressure
$p_{\mathrm{rms}}{}^{(e)}$	root-mean-square wall pressure in elastic pipe
$p_{\mathrm{rms}}^{(r)}$	root-mean-square wall pressure in rigid pipe
$(p_{\mathrm{rms}})_{\max}$	maximum pressure p_{rms}
$(p_{\mathrm{rms}}^{(e)})_{\max}$	maximum pressure $p_{\mathrm{rms}}^{(e)}$
$(p_{\mathrm{rms}}^{(r)})_{\max}$	maximum pressure $p_{\mathrm{rms}}^{(r)}$
$(p_{\mathrm{rms}}^{(r)})_{\min}$	minimum pressure $p_{\mathrm{rms}}^{(r)}$
p_t	wall pressure fluctuations
Q	water volume
Re_D	flow Reynolds number
Re_d	jet Reynolds number
S	narrowing severity
T	analyser acquisition time
t	time
U	mean axial flow velocity in pipe
u	mean axial flow velocity in narrowing
u_c	convective velocity
z	axial coordinate
ν	kinematical viscosity of fluid
ς	relative deflection coefficient
ρ	mass density of fluid
τ	time delay
ω	circular frequency

invasive, involves a risk of infection, bleeding and arrhythmia, etc. and is usually only used when a stenosis results in serious clinical symptoms (Mirolyubov, 1983; Young, 1979).

In such a situation, developing *non-invasive* diagnostic methods for finding a stenosis from an analysis of changes in the hydrodynamic and/or acoustic characteristics of the associated blood flow is of great concern to the medical clinician. The method of passive location of the sound field produced by a stenosis (or phonoangiography) occupies a special place among such techniques (Duncan et al., 1975; Lees and Dewey, 1970; Pitts and Dewey, 1979). It requires the availability of complete and reliable information about the fundamental mechanisms of vascular sound generation and transmission to the body surface, as well as the various factors which affect them (these include the rheological properties of the fluid, the character and structure of the flow in the vessel, the physical and geometrical characteristics of the relevant vascular district and stenotic obstruction, the structure and acoustical properties of the human body, etc.).

With these known, a model of the appropriate vascular district can be developed and used to predict the relationship between the characteristics of the sound field heard at the body surface and the parameters of the vessel and the flow. These relationships can then be applied to solve the inverse problem (namely, finding a stenosis from the corresponding changes in the acoustic field structure).

An adequate description of the flow and the noise sources (i.e., the wall pressure fluctuations, p_t) behind a stenotic narrowing is one of the key factors in the method of phonoangiography. As analysis of the scientific literature shows, the spatial structure of both the flow and the pressure p_t behind narrowings of the simplest shapes has been investigated rather well. In particular, the disturbed flow region immediately behind a narrowing has been found. It has been characterised as follows. First, a separation region (with recirculating flow between the jet and the vessel wall) is usually observed. It is followed by a reattachment region, and finally by flow stabilization and recovery to the state upstream of the narrowing (Borisyuk, 2002; Clark, 1977; Mirolyubov, 1983; Young, 1979). The flow centerline velocity in the flow separation and flow reattachment domains remains practically like that in the narrowing (Abdallah and Hwang, 1988; Borisyuk, 2002; Clark, 1977; Giddens et al., 1976; Mirolyubov, 1983; Young, 1979). The rms (i.e., root-mean-square) wall pressure is characterised by a sharp increase in these domains, and reaches a maximum before the flow reattachment point (Clark, 1977; Fredberg, 1977; Mirolyubov, 1983; Tobin and Chang, 1976; Young, 1979). There are also approximate estimates for the upper limits of the longitudinal dimensions of the flow regions identified above, as well as quantitative relationships relating both the distance from a narrowing to the point of maximum rms wall pressure and

the rms pressure magnitude at this point to the parameters of the flow, vessel and narrowing (Clark, 1977; Fredberg, 1977; Tobin and Chang, 1976). However, the appropriate estimates and relationships of different authors differ from each other, even for identical narrowing geometries [compare, for example, the appropriate estimates and relationships given in the works of Clark (1977), Fredberg (1977), Mirolyubov (1983), Tobin and Chang (1976), Young (1979)].

Unlike the spatial characteristics of the wall pressure fluctuations behind a narrowing, the spectral characteristics of the pressure p_t have been investigated rather little. A few works can be found (Berger and Jou, 2000; Clark, 1977; Fredberg, 1977; Kim and Corcoran, 1974; Mirolyubov, 1983; Tobin and Chang, 1976; Young, 1979), in which only the general shape of the wall pressure power spectrum has been obtained, and the qualitative dependence of the spectrum level on the flow Reynolds number and the narrowing severity has been analysed. More specific features of the spectrum (such as local maxima, slope of the spectral curve, etc.) and their relation to the vortex structures behind a narrowing, as well as variation of the spectrum with axial distance from the narrowing were either not found or given insufficient attention by investigators. However, these details are important for analysis of the corresponding acoustic field (Borisyuk, 1998, 1999, 2002, 2003). Furthermore, no studies of the effect of vessel wall elasticity and narrowing length on the wall pressure characteristics are available.

The lack of information about the spectral structure of the wall pressure fluctuation field, the effect of the vessel wall elasticity, and the influence of narrowing length, as well as the absence of universal estimates and relationships for the spatial characteristics of the pressure field, stimulated this investigation. The paper begins with a description of the experimental system, and a discussion of the considerations and assumptions made in its development (Section 2). The results of this study for the pressure fluctuations in rigid and elastic pipes behind an axisymmetric narrowing are analysed in Section 3. Here two mean statistical characteristics of the field p_t—namely, its rms value, p_{rms}, (Section 3.1) and the power spectrum, P, (Section 3.2)—are considered, and the effects of the narrowing severity and length, as well as the flow Reynolds number, the pipe wall elasticity and the axial distance from the narrowing are studied. The discussion is organized so that initially the data for a rigid pipe are analysed (in Section 3.1.1 for p_{rms}, in Section 3.2.1 for P). Then these data are used as a basis for comparison in the analysis of the corresponding measurements for an elastic pipe (Sections 3.1.2 and 3.2.2). The practical implications of the results of this work are discussed in Section 3.3. Then the conclusions of the investigation are set out (Section 4) and acknowledgements given. Finally, a list of the literature cited is presented.

2. Experiment

Precise modelling of the stenosed region of a larger blood vessel and the flow in it is difficult. However, noting that the characteristic flow scales and the region's dimensions are small compared with the acoustic wavelengths of interest in vascular stenosis murmurs, it is possible to make simplifying assumptions. Under these assumptions, the basic elements of the vascular district under investigation can be simulated quite well within acceptable accuracy limits. As a result, the basic *in vitro* flow and wall pressure fluctuation characteristics will be similar to their counterparts *in vivo*.

Taking these arguments into account, a suitable experimental system has been developed. A schematic of this system and its test-section is shown in Figs. 1 and 2, respectively. Here the basic elements are:

(i) the upper supply and the lower collection reservoirs;
(ii) cut silicone elastic pipe, of inner diameter $D = 18$ mm and wall bending stiffness coefficient $D_v^{(e)} = 1.2 \times 10^{-4}$ N m, representing a larger blood vessel (the other pipe and vessel parameters are given in Table 1);

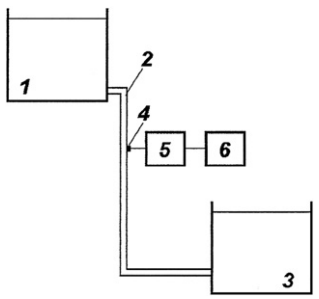

Fig. 1. Schematic of experimental system: 1—supply reservoir; 2—silicone pipe; 3—collection reservoir; 4—pressure sensor; 5—amplifier; 6—frequency analyser.

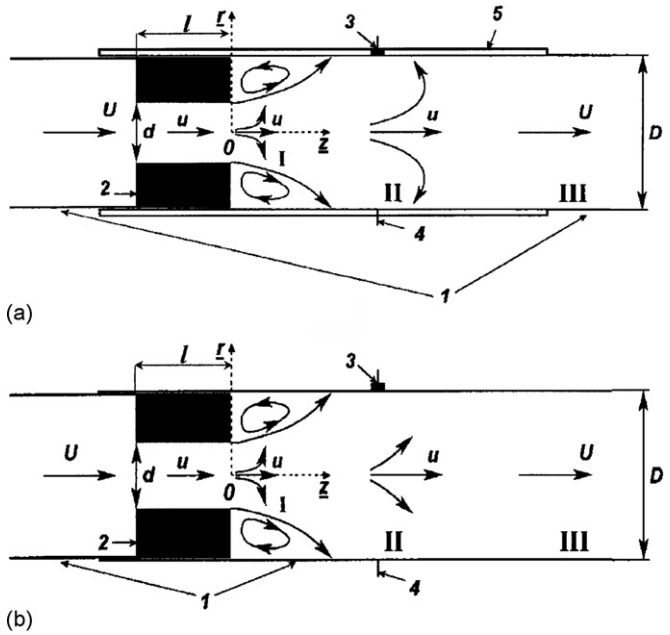

Fig. 2. Schematic of test-section with a rigid (a) and an elastic (b) measuring block: 1—silicone pipe; 2—insertion; 3—pressure sensor; 4—needle for dye injection; 5—rigid transparent glass pipe; I—flow separation region; II—flow reattachment region; III—region of flow stabilization and redevelopment into the state upstream of the insertion.

(iii) a set of hollow, rigid-walled, abrupt axisymmetric cylinders, of inner diameter d and length l, which are inserted into the elastic pipe and simulate stenoses (d and l have values ranging from 6 mm to 16 mm and from 5 mm to 50 mm, respectively, with steps of 1 mm).

(iv) the movable measuring block having either a rigid or an elastic wall; the rigid-walled block (see Fig. 2(a)) consists of a transparent glass pipe (of length 80 cm,[1] inner diameter D[2] and wall bending stiffness coefficient $D_v^{(r)} = 5.25 \times 10^{-3}$ N m) with a pressure transducer and a needle (for dye injection) flush-mounted into the pipe wall opposite one another; the elastic-walled block (see Fig. 2(b)) is a segment of the silicone pipe (with pressure sensor and needle inserted similarly) located immediately behind a cylindrical insertion. The pressure sensor has sensing surface diameter 1.2 mm,[3] and sensitivity 6 μV/Pa (Voskoboinik et al., 2000, 2002).

The working medium was water at an indoor temperature (unless otherwise stated, hereinafter the indices "e" and "r" indicate the elastic and rigid wall, respectively).

The following considerations were used in developing the test-section of the experiment.

Larger blood vessel: Larger blood vessels can be considered as elastic thin-walled pipes having an inner diameter of approximately 0.1–2.0 cm and a wall thickness–diameter ratio of approximately 0.04–0.13 (Berger and Jou, 2000;

[1]This length was chosen to have, on the one hand, an effectively infinite rigid pipe when viewed from the measurement location, and, on the other hand, enough rigid wall downstream of the insertion to allow the corresponding measurements in the total disturbed flow region. In fact, for the flow velocities, insertion parameter values and measurement position (at least 40 cm upstream of the end of the rigid pipe) used in this experiment, the flow in the pipe with and without insertion took at least 0.1 s and 1 s, respectively, to cover the distance from the upper pipe end to the measurement point and from the measurement point to the lower pipe end. This time greatly exceeds the maximum period of the disturbed flow fluctuations due to an insertion, which allows one to consider the rigid pipe as effectively infinite. Also, for this choice of measurement point, it was possible to make measurements on a rigid wall in the total disturbed flow region whose length did not exceed $12D = 21.6$ cm (see Section 3.1.1).

[2]In using the rigid-walled block, the outer diameter of the insertion, D, and the elastic pipe wall thickness over the insertion were reduced in such a way to allow movement of the rigid pipe over the elastic one and the insertion, and to avoid water leakage between the pipes.

[3]For the flow speeds and insertion parameter values used in this experiment, the effects of spatial averaging by this sensor were important for frequencies above approximately 800 Hz (Voskoboinik et al., 2000, 2002). However, in this frequency range the measured signal was dominated by background noise.

Table 1
Parameters of the pipes and a larger blood vessel.

Type of pipe	Diameter (mm)	Wall thickness (mm)	Wall thickness/ diameter ratio	Modulus of elasticity (N/m^2)	Poisson's ratio
Silicone	18	2	0.111	1.5×10^5	0.41
Glass	18	2	0.111	7.8×10^6	0.1
Blood vessel	1–20	0.04–2.6	0.04–0.13	$(1.29–10) \times 10^5$	0.23–0.57

Borisyuk, 1998, 1999, 2002, 2003; Iudicello et al., 1997; Mirolyubov, 1983; Wang et al., 1990; Young, 1979). The silicone elastic pipe used in the experiment satisfies these conditions. In addition, the choice of this pipe as a model of a larger blood vessel is because it allows close matching of other geometrical and physical parameters (see Table 1), and also because silicone pipes are widely used as a mechanical analogue of blood vessels in *in vitro* studies (Borisyuk, 2002; Iudicello et al., 1997; Kirkeeide et al., 1977). The use of the rigid-walled measuring block is for two reasons. Firstly, since the effect of the vessel wall elasticity on the pressure p_t is studied here, it is necessary to have reference data for a rigid wall to be compared with the appropriate data obtained on an elastic surface. Secondly, rigid-walled measuring blocks are used by many researchers in studying the wall pressure fluctuations behind a vessel narrowing [see, for example, Berger and Jou (2000), Clark (1977), Fredberg (1977), Giddens et al. (1976), Kim and Corcoran (1974), Mirolyubov (1983), Tobin and Chang (1976), Young (1979)], and therefore it facilitates comparison with their data. Apart from helping to fulfil the aims stated in the Introduction, such a comparison will provide information on the reliability of the measurements made in this experiment.

Stenosis: The stenosis is simulated by a hollow, rigid-walled, abrupt axisymmetric cylinder. Such a representation is justified by the fact that the wall of an arterial stenosis has high stiffness compared with that of the vessel proximal and distal to it, due to calcification (Berger and Jou, 2000; Borisyuk, 2002; Clark, 1977; Fredberg, 1977; Iudicello et al., 1997; Mirolyubov, 1983; Young, 1979). As for the axisymmetric, abrupt, cylindrical geometry[4] of a plug, this is the simplest narrowing shape that allows one to study the role of its most important geometrical characteristics: minimum cross-sectional area (or narrowing severity) and length. In addition, with such an idealization, one can obtain flow energy distributions behind the narrowing which, in general, appear similar to those observable behind real stenotic geometries.

Blood: A typical blood substitute in *in vitro* experiments is water at indoor temperature. Such a replacement is made in this study. This is because the mass density and the sound speed of normal blood are approximately $1050\,kg/m^3$ and 1500 m/s, respectively (Berger and Jou, 2000; Mirolyubov, 1983; Young, 1979), which are very close to those of water. Another reason is that blood is usually considered to be an incompressible, homogeneous and (at high shear rates above $50\,s^{-1}$, commonly found in the larger arteries) Newtonian fluid[5] (Mirolyubov, 1983; Young, 1979). The difference in viscosity between water and blood is compensated for by the choice of flow velocities at which the blood and water flows are similar in the relevant Reynolds number.

Flow: In this work, the quasi-steady approximation to real blood flow is made. This is because the blood flow rate during the cardiac cycle is a slowly varying function compared with the disturbed flow parameter fluctuations due to a stenosis. Indeed, the cardiac cycle and the blood-flow-rate frequencies are of the order of 1 Hz, whereas the frequencies of the fluctuations usually lie between 20 Hz and 1 kHz. Nonetheless, there is a difference between the wall pressure behind a narrowing in quasi-steady and pulsating flow (according to the literature [see, for example, Bluestein and Einav (1995)], the pulsating blood flow plays a major role by suppressing the fluctuations during the diastolic phase); this will be investigated at a future stage of modelling real blood flow in stenosed vessels. For the moment one can say that the influence of this difference on the mean statistical characteristics that are considered in this study will be significantly smoothed out due to averaging, and it will be a higher-order effect compared with the influence of more fundamental parameters, such as the Reynolds number and the narrowing diameter and length.

The experimental system was operated in the following way. Due to the difference between the water levels in the supply and collection reservoirs, a flow with controlled characteristics was created in the silicone pipe. The flow became

[4]The results for other, more realistic narrowings (in particular, various more streamlined axisymmetric geometries, as well as non-axisymmetric geometries, including one-sided ones), which are available in the scientific literature and have also been obtained in this series of experiments, will be presented in a subsequent paper.

[5]Strictly speaking, the latter assumption is less justifiable than the former two. However, since the effect of non-Newtonian blood behaviour on the wall pressure fluctuations behind a vessel narrowing is not a subject of this study, here it is conjectured that the discrepancy between Newtonian water and non-Newtonian blood can be neglected.

disturbed in the narrowing (insertion) and then remained disturbed in a finite region behind it (see Fig. 2). In this region were the flow separation (I) and flow reattachment (II) zones. Then flow stabilization and recovery back to the state upstream of the narrowing were observed (zone III). The wall pressure fluctuations, p_t, were measured in all these zones, and their statistical characteristics studied.

The connection of the silicone pipe and the measuring block was such that, on the one hand, it did not cause additional flow disturbances, and, on the other hand, allowed the block to be moved along and rotated about its axis. As a result, it was possible to make measurements at different values of the axial and/or angular coordinates. Mild dye injection via the needle situated just opposite the pressure transducer allowed one to determine both the location of the flow reattachment point and the position of the pressure transducer (i.e., the measurement point) relative to it.

The mean axial flow velocity, U, was determined from the ratio of the water volume, Q, accumulated in the collection tank (calibrated in litres) during the period T of data acquisition to the cross-sectional area of the pipe, $\pi D^2/4$, and the time T,[6] viz.

$$U = \frac{Q}{T\pi D^2/4}.$$

The mean axial flow velocity in the narrowing, u, was found from the mass conservation condition in the narrowed and normal segments of the pipe, viz.

$$u = U\left(\frac{D}{d}\right)^2.$$

In order to have similarity in the flow Reynolds number, $\mathrm{Re}_D = UD/\nu$ (where ν is the kinematical fluid viscosity) between the experimental flow and real blood flow in a larger vessel, only velocities $U < 0.39$ m/s were considered in the experiment. For this velocity range, Re_D was below 7000, which is typical of the larger arteries of the human body, such as the ascending aorta and the carotid and femoral arteries (Berger and Jou, 2000; Borisyuk, 1998, 1999, 2002, 2003; Clark, 1977; Kim and Corcoran, 1974; Kirkeeide et al., 1977; Mirolyubov, 1983; Tobin and Chang, 1976; Young, 1979).

3. Results

As in many previous cases [see, for example, Berger and Jou (2000), Clark (1977), Fredberg (1977), Kim and Corcoran (1974), Mirolyubov (1983), Pedrizzetti (1996), Tobin and Chang (1976), Young (1979)], the axisymmetric geometry and coaxial location of the pipes and cylindrical insertion resulted in axial symmetry (to a first approximation) of the test section flow and, hence, axial symmetry of the wall pressure fluctuation field, p_t. This property of the field p_t has been verified by comparison of the corresponding data recorded at different angles but the same axial location. It should, however, be noted that this comparison has only been made for the two mean statistical characteristics of the random field p_t which are typically chosen in studying the field structure behind a vessel narrowing (see, for example, the above references). These are the rms pressure,

$$p_{\mathrm{rms}} = \sqrt{\langle p_t^2 \rangle},$$

where the brackets $\langle \ldots \rangle$ denote an ensemble average, and the power spectrum, $P(f)$, which is defined as (Blake, 1986; Borisyuk and Grinchenko, 1997)

$$P(f) = 4\pi P(\omega), \quad P(\omega) = \frac{1}{2\pi}\int_{-\infty}^{\infty} < p_t(t) p_t(t+\tau) > \mathrm{e}^{\mathrm{i}\omega\tau}\,\mathrm{d}\tau;$$

here f is the frequency, ω the circular frequency, t the time, and τ the time delay.

[6]The period T was fixed by the frequency analyser settings. In this experiment, it was equal to 4 s, 8 s or 16 s. During this time the difference between the levels of water in upper and lower reservoirs, H, changed negligibly (the change in H, ΔH, was less than 14 mm, which is less than 1% of its relative value, $\Delta H/H$). In such a situation, the experimental flow could thus be considered quasi-steady with axial velocity, given by its mean value, U.

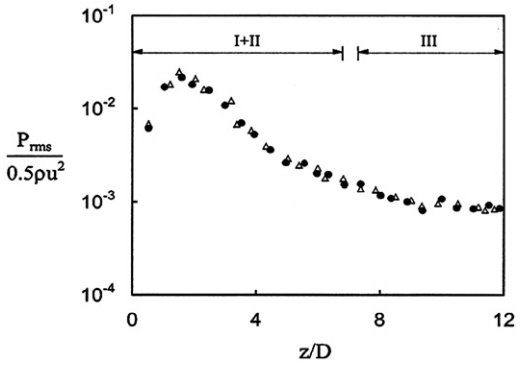

Fig. 3. Axial distribution of the pressure p_{rms} behind a pipe narrowing ($d=9$ mm, $S=75\%$, $l=20$ mm, $U=0.25$ m/s, $\mathrm{Re}_D=4500$): ●, rigid pipe, △, elastic pipe.

3.1. Root-mean-square wall pressure

Fig. 3 presents typical axial distributions of the rms wall pressure immediately behind an insertion in rigid and elastic pipes. Both measurements were made behind the insertion of the same severity, S, quantified here as

$$S=\left(1-\frac{d^2}{D^2}\right)\times 100\%,$$

and the same length, l, and at the same value of the flow Reynolds number, Re_D.

3.1.1. Pressure p_{rms} in a rigid pipe

Study of the axial variation of the rms wall pressure in a rigid pipe, $p^{(r)}_{\mathrm{rms}}$, depicted in Fig. 3, shows that it initially increases sharply as the distance from the narrowing increases, reaching a maximum, $(p^{(r)}_{\mathrm{rms}})_{\max}$, at the point $z=L^{(r)}_{\max}$ (this range of z is included in the most disturbed flow region I+II)). Then the rms pressure decreases rather rapidly and, at the very end of the flow stabilization region III, it reaches a minimum, $(p^{(r)}_{\mathrm{rms}})_{\min}$, which is equal to the value measured upstream of the narrowing. The length $L_{\mathrm{I+II}}$ of the region I+II can be seen from Fig. 3 not to exceed approximately seven pipe diameters viz.

$$L_{\mathrm{I+II}}<7D.$$

The axial dimension $L_{\mathrm{I+II+III}}$ of the total disturbed flow region I+II+III is less than $12D$, viz.[7]

$$L_{\mathrm{I+II+III}}<12D.$$

Similar estimates for the longitudinal dimensions of the domains I+II and I+II+III have been obtained for the other experimental parameter values. They also agree with the corresponding data of Mirolyubov (1983) and Young (1979), who give the same values for the upper limits of the lengths $L_{\mathrm{I+II}}$ and $L_{\mathrm{I+II+III}}$.

Analysis of the rms wall pressure and the location of its maximum behind insertions of the same length, l, and different severity ($20\%<S<89\%$) and/or at various values of the flow Reynolds number ($\mathrm{Re}_D<7000$) shows that:

(a) this maximum always lies between the insertion and the flow reattachment point in the range $z/D\approx 1.3$–2.6, and moves downstream/upstream as S and(or) Re_D increase/decrease;
(b) an increase/decrease in S and(or) Re_D causes a general increase/decrease of the local disturbed flow energy and, hence, a corresponding general increase/decrease (ranging from a few percents to a few times depending on the measurement position, z, and the compared values of S and(or) Re_D) of the pressure $p^{(r)}_{\mathrm{rms}}$.

[7] In obtaining these estimates and similar estimates for an elastic pipe (see Section 3.1.2), the downstream ends of the regions I+II and I+II+III were determined from the conditions $(p_{\mathrm{rms}}-(p_{\mathrm{rms}})_{\min})/(p_{\mathrm{rms}})_{\min}=0.3$ and $|p_{\mathrm{rms}}-(p_{\mathrm{rms}})_{\min}|/(p_{\mathrm{rms}})_{\min}=0.01$, respectively.

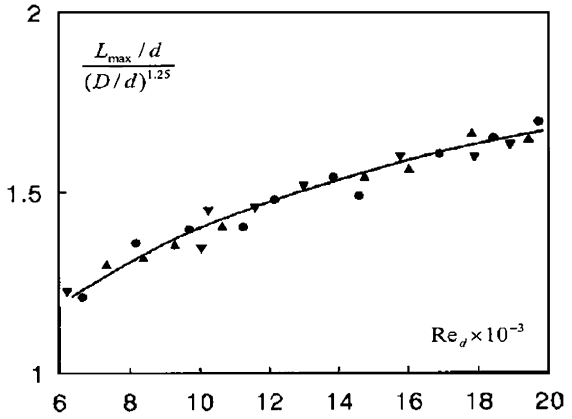

Fig. 4. Dependence of distance L_{max} on the jet Reynolds number, Re_d, and the diameter ratio, D/d, in a rigid pipe: ▲, $S = 55.56\%$ ($d = 12$ mm); ●, $S = 75\%$ ($d = 9$ mm); ▼, $S = 88.89\%$ ($d = 6$ mm); solid line, $0.127(Re_d)^{0.26}$.

Similar results have been obtained by Clark (1977) and Tobin and Chang (1976).[8]

Variations in the rms pressure caused by changes in the narrowing length, l, are much weaker than those due to changes in the severity S and/or the Reynolds number Re_D. More specifically, they are generally in that a significant (i.e., around 50%) increase/decrease in l from the value of 20 mm [9] (for approximately $S > 69\%$ and $Re_D > 1400$ [10]) results in:

(i) an insignificant (i.e., of the order of 5–7% depending on S and(or) Re_D) shift of the point $z = L_{max}^{(r)}$ downstream/upstream;
(ii) an increase/decrease of the flow energy dissipation in the narrowing (due to the increase/decrease of the viscous forces there) and, consequently, a small (i.e., of the order of 5–10% depending on z, S and(or) Re_D) decrease/increase of the rms pressure.

In order to characterise quantitatively the dependence of the distance $L_{max}^{(r)}$ on the narrowing severity and the jet Reynolds number, $Re_d = ud/\nu$, it was assumed to take the form

$$\frac{L_{max}^{(r)}}{d} = \alpha(Re_d)^{\beta}\left(\frac{D}{d}\right)^{\gamma}. \tag{1}$$

In varying the parameters α, β and γ in expression (1), it was found that the data for narrowings of differing severities could be reduced to approximately a single curve with the values $\alpha = 0.127$, $\beta = 0.26$, $\gamma = 1.25$, as shown in Fig. 4. The relative error coefficient ç, calculated from the expression

$$\varsigma = \frac{\sum_{i=1}^{N}}{N}\varsigma_i, \quad \varsigma_i = \left|1 - \frac{\alpha(Re_d)^{\beta}(D/d)^{\gamma}}{L_{max}^{(r)}/d}\right|_{Re_d = (Re_d)_i},$$

where N is the number of measurements, was equal to 0.115. This indicates a small difference between the experimental values for the distance $L_{max}^{(r)}$ and those found from formula (1). Consequently, one can conclude that

$$\frac{L_{max}^{(r)}}{d} \approx 0.127(Re_d)^{0.26}\left(\frac{D}{d}\right)^{1.25}, \tag{2a}$$

[8]Clark gives the range 1.3–2.5 for the dimensionless location of the maximum, $L_{max}^{(r)}/D$, whereas Tobin and Chang state 1.5–2.5.

[9]The case of the critical value, $l = l_{cr}$, at which the narrowing length can be considered to be effectively infinite, and further increases have no effect on the wall pressure, is discussed in Section 3.3.

[10]At lower values of S and Re_D the investigated magnitude was even less sensitive to the indicated change of l.

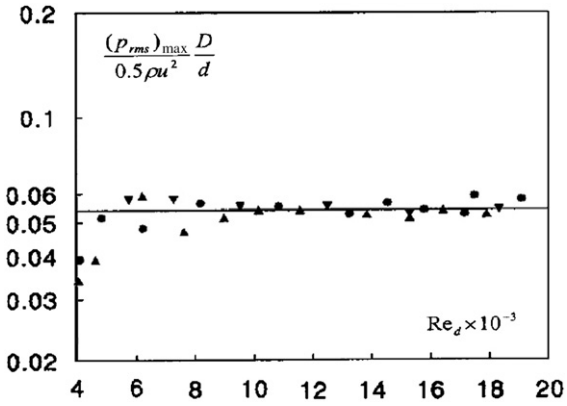

Fig. 5. Maximum pressure $(p_{rms})_{max}$ for insertions of differing severity, S, and different values of the jet Reynolds number, Re_d, in a rigid pipe: ▲, $S = 55.56\%$ ($d = 12$ mm); ●, $S = 75\%$ ($d = 9$ mm); ▼, $S = 88.89\%$ ($d = 6$ mm); solid line, 0.054 level.

or

$$\frac{L^{(r)}_{max}}{D} \approx 0.127(\mathrm{Re}_d)^{0.26}\left(\frac{D}{d}\right)^{0.25}. \tag{2b}$$

Estimates (2a) and (2b) for the distance $L^{(r)}_{max}$ indicate that the point of the maximum r.m.s wall pressure shifts to the right/left as the jet Reynolds number and(or) the narrowing severity increase/decrease. This agrees well with the qualitative effects of these parameters noted above and found by Clark (1977), Mirolyubov (1983), Tobin and Chang (1976) and Young (1979). However, estimates (2a) and (2b) differ slightly from the corresponding quantitative estimates of Clark (1977) in the values of the coefficients α, β and γ (Clark gives $\alpha = 0.115$, $\beta = 0.27$, $\gamma = 1.26$).[11]

Study of the maximum pressure, $(p^{(r)}_{rms})_{max}$, shows that (like the rms pressure throughout the flow domain under investigation) it increases/decreases as S and(or) Re_d increase/decrease. Furthermore, for jet Reynolds numbers exceeding 8500, it is approximately proportional to the jet dynamic pressure, $\rho u^2/2$, and the ratio of the diameters of the narrowed and normal segments of the pipe, d/D, viz. (Fig. 5)

$$\frac{\left(p^{(r)}_{rms}\right)_{max}}{0.5\rho u^2}\frac{D}{d} \approx 0.054, \quad \mathrm{Re}_d > 8500. \tag{3}$$

Expression (3) differs from the corresponding quantitative estimates obtained by Clark (1977) and Tobin and Chang (1976). Clark's expression is

$$\frac{\left(p^{(r)}_{rms}\right)_{max}}{0.5\rho u^2}\frac{D}{d} \approx \begin{cases} 0.06, & \mathrm{Re}_d \geq 10\,000, \\ 0.088, & \mathrm{Re}_d \geq 16\,000, \end{cases}$$

whereas Tobin and Chang give

$$\frac{\left(p^{(r)}_{rms}\right)_{max}}{0.5\rho u^2}\frac{D}{d} \approx 0.071$$

without indication of the range for Re_d.

[11] From estimates (2a) and (2b) it also follows that when the velocity U and the diameter d are changed in such a way that the ratio U/d^2 is held constant, the jet velocity, $u = U(D/d)^2$, remains constant, and the length $L^{(r)}_{max}$ becomes effectively independent of d (i.e., $L^{(r)}_{max} \approx 0.127(u/\nu)^{0.26}D^{1.25}d^{0.01}$). A similar conclusion can be reached from the analysis of the corresponding quantitative estimates of Clark (1977).

3.1.2. Pressure p_{rms} in an elastic pipe

Analysis of the axial distribution of the rms wall pressure behind an insertion in an elastic pipe, $p^{(e)}_{\mathrm{rms}}$ (see Fig. 3) shows that in general it looks like that in a rigid pipe. In particular, the shapes of the distributions $p^{(e)}_{\mathrm{rms}}$ and $p^{(r)}_{\mathrm{rms}}$ are similar, and the locations of their maxima, $z=L^{(e)}_{\max}$ and $z=L^{(r)}_{\max}$, are close to each other. Also the lengths of the regions I+II and I+II+III in an elastic pipe are practically equal to those in a rigid pipe.[7] In contrast, the amplitude of $p^{(e)}_{\mathrm{rms}}$ is generally slightly higher[12] than that of $p^{(r)}_{\mathrm{rms}}$. However, for the pipes and the velocity range used in the experiment, this only becomes noticeable (i.e. approximately 5–13% of increase of relative difference, $\left(p^{(e)}_{\mathrm{rms}}-p^{(r)}_{\mathrm{rms}}\right)/p^{(r)}_{\mathrm{rms}}\times 100\%$, depending on measurement position, narrowing severity and Reynolds number[13]) approximately for $S\geq 75\%$ and $\mathrm{Re}_d\geq 9000$.

Analysis of variations in the pressure $p^{(e)}_{\mathrm{rms}}$ caused by changes in the narrowing severity and/or length, as well as the flow Reynolds number shows that generally they are similar to the rigid-wall case (this includes both the range of variation of the distance from the narrowing to the point of maximum rms wall pressure and the behaviour of this distance with S, l and/or Re_D).

Study of the quantitative dependence of the distance $L^{(e)}_{\max}$ on the experimental parameters shows that it is close to the rigid pipe result (see formulas (2a) and (2b)), viz.

$$\frac{L^{(e)}_{\max}}{d}\approx \alpha(\mathrm{Re}_d)^{0.26}\left(\frac{D}{d}\right)^{1.25},\quad \frac{L^{(e)}_{\max}}{D}\approx \alpha(\mathrm{Re}_d)^{0.26}\left(\frac{D}{d}\right)^{0.25}. \tag{4}$$

The only difference between expressions (4) and (2a), (2b) is in the values of the coefficient α. In the rigid pipe α is approximately equal to 0.127, whereas in the elastic pipe (within the same variation ranges of the flow and narrowing characteristics) its values lie between 0.119 and 0.124 (a conclusion concerning the dependence of α on the pipe wall properties, etc. may be deduced after carrying out the appropriate experiments with elastic pipes having different wall properties).

The quantitative estimate for the maximum pressure $\left(p^{(e)}_{\mathrm{rms}}\right)_{\max}$ at the point $z=L^{(e)}_{\max}$ is also similar to the rigid surface expression (see formula (3)), viz.

$$\frac{\left(p^{(e)}_{\mathrm{rms}}\right)_{\max}}{0.5\rho u^2}\frac{D}{d}\approx K,\quad \mathrm{Re}_d>9000. \tag{5}$$

However, two differences should be mentioned. Firstly, the maximum pressure in the elastic pipe only becomes approximately proportional to the jet dynamic pressure and the diameter ratio of the narrowed and normal segments of the pipe from $\mathrm{Re}_d\approx 9000$ (instead of $\mathrm{Re}_d\approx 8500$ in the rigid pipe). Secondly, the coefficient K in expression (5) falls in the range 0.059–0.061, whereas in estimate (3) K is approximately equal to 0.054 (obtaining of a functional dependence of K on the pipe wall properties, etc. requires carrying out extensive series of additional experiments).

3.2. Power spectrum of the wall pressure fluctuations

Typical results for the power spectra of the wall pressure fluctuations in rigid and elastic pipes are presented in Fig. 6. Both recordings were made in the flow separation I (see Fig. 6(a)) and flow reattachment II (see Fig. 6(b)) regions[14] at the same values of the parameter set S, l and Re_D.

[12]In making each series of the recordings, there were some locations at the very end of the region I+II and in the region III where the r.m.s. wall pressure either practically did not change or even slightly decreased with the chosen decrease in the pipe wall bending stiffness ($D^{(r)}_v/D^{(e)}_v=43.75$). A convincing explanation of this effect cannot yet be given. However, it might be due to measurement errors.

[13]The other conditions being equal, the difference increases/decreases with an increase/decrease of S and(or) Re_D.

[14]Recordings of the power spectrum in the region III are not presented in this paper. This is because we are concerned with wall pressure fluctuations as noise sources for non-invasive acoustic diagnosis. The intensity of these sources, p_t^2, in region III is much lower than that in region I+II (for example, from Fig. 3 it follows that the value p_t^2 in domain III is approximately 2–3 orders of magnitude lower than in domain I+II; in terms of the power spectrum this is about 20–30 dB difference in levels). Hence, the total noise field produced by the flow region I+II+III will be dominated by the contribution from the flow region I+II. Consequently, for acoustic purposes, region III is of secondary importance compared with region I+II.

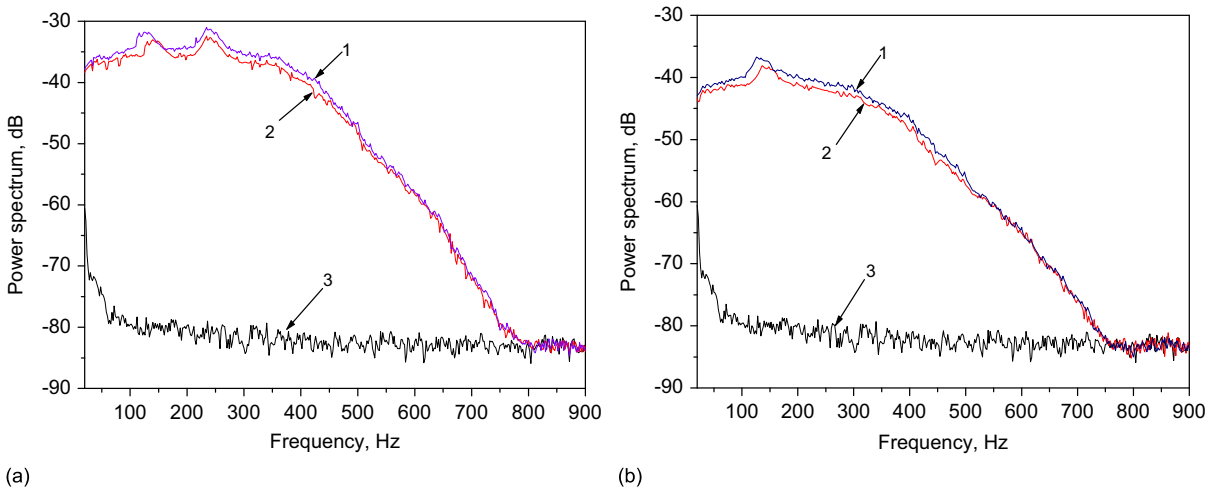

Fig. 6. Power spectrum of the wall pressure fluctuations at the points (a) $z = L_{max}$ and (b) $z = 4D$ behind the insertion ($d = 10$ mm, $S = 69.14\%$, $l = 20$ mm) at a mean flow velocity $U = 0.35$ m/s ($Re_D = 6300$): 1—elastic pipe; 2—rigid pipe; 3—background noise.

3.2.1. Power spectrum of the wall pressure fluctuations in a rigid pipe

Study of the power spectrum in a rigid pipe, P_r (see curve 2 in Figs. 6(a) and (b)) shows that generally, in both flow regions, it looks like that of the wall pressure fluctuations in fully-developed turbulent flow in a rigid pipe without narrowing, P_0 (Blake, 1986; Borisyuk and Grinchenko, 1997). More specifically, the low-frequency domain of the spectrum P_r in each flow region is the energy-containing and characterizes the distribution of the disturbed flow energy among the energy-containing large-scale eddies in that region. The high-frequency domain of the spectrum P_r corresponds to small-scale eddies which contain a small part of the disturbed flow energy. As a result, here the level is much lower than in the low-frequency domain and decreases rapidly as the frequency increases (corresponding to the decrease in a vortex' energy with the decrease of its size).

A characteristic feature of the spectrum P_r (compared with P_0, which is a rather smooth function) is that it has local pronounced low-frequency maxima (two in Fig. 6(a) and one in Fig. 6(b)). Analysis of the flow structure (see Fig. 2) and the flow energy distribution among the eddies behind the narrowing shows that these maxima are determined by the corresponding large-scale vortex formations in the flow separation and flow reattachment regions, and that the frequencies of the maxima can be attributed to the characteristic frequencies of the vortex formations, namely:

(i) in region I, these are eddies with sizes of order $d/2$, which move at speeds of order u in the jet and are characterized by frequencies of order

$$f_{ch}^{(1)} = \frac{2u}{d} = \frac{2UD^2}{d^3}, \tag{6}$$

and eddies with scales of order $h = (D-d)/2$ in the recirculating flow region between the jet and the pipe wall, which have frequencies of order

$$f_{ch}^{(2)} = \frac{u_c}{h}, \tag{7}$$

where $u_c \sim 0.45u - 0.6u$ is a convection velocity on the outer side of the jet (Abdallah and Hwang, 1988; Borisyuk, 2002);

(ii) in region II, these are vortex formations with sizes of order $D/2$ which are convected at speeds of order u and have frequencies of order

$$f_{ch}^{(3)} = \frac{2u}{D} = \frac{2UD}{d^2}. \tag{8}$$

Table 2
Frequency ranges of the pronounced low-frequency maxima in the spectrum P_r in Fig. 6 and values of the corresponding frequencies (6)–(8), Hz.

Fig. 6(a)	Fig. 6(a)	Fig. 6(b)
$126<f<164$	$220<f<266$	$122<f<166$
$f_{ch}^{(2)}$ in the range 127.6–170.1	$f_{ch}^{(1)}=226.8$	$f_{ch}^{(3)}=126$

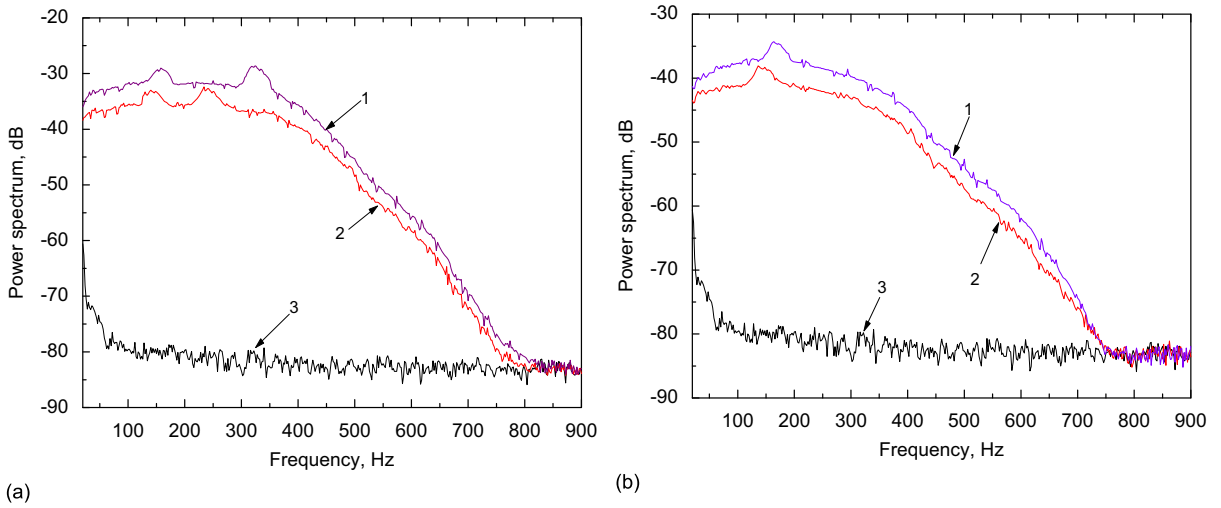

Fig. 7. Power spectrum of the wall pressure fluctuations in a rigid pipe, P_r, at the points (a) $z=L_{\max}^{(r)}$ and (b) $z=4D$ at a mean flow velocity $U=0.35$ m/s ($\mathrm{Re}_D=6300$): 1—insertion ($d=9$ mm, $S=75\%$, $l=20$ mm); 2—insertion ($d=10$ mm, $S=69.14\%$, $l=20$mm); 3—background noise.

The aforesaid was verified in two ways. On the one hand, the characteristic frequencies (6)–(8) were calculated and compared with the frequencies of the corresponding pronounced maxima in the spectrum P_r. The correlation between the theoretical and experimental data was rather good (see Table 2; it was similar for the other values of the narrowing and flow parameters). On the other hand, a small grid (with square holes of dimensions less than $d/3\times d/3$) was inserted in the outlet section of the pipe narrowing. The grid was expected to destroy the large-scale vortex structures both in the jet and the flow region II, as well as change the structure and dimensions of the recirculating flow region. This should have resulted in the disappearance of the maxima in the spectrum P_r at the frequencies $f_{ch}^{(1)}$, …, $f_{ch}^{(3)}$. This effect was indeed observed in the experiment.

As noted in the Introduction, it appears that the variation of the wall pressure power spectrum with axial distance from the narrowing has not previously been studied. Comparative analysis of the spectra recorded here at different values of the axial coordinate shows that (compare, for example, the corresponding curves in Figs. 6(a) and (b)):

(i) the local disturbed flow energy decreases as the distance from the narrowing increases, which results in a general decrease in the spectrum level;
(ii) the disturbed flow structure (see Fig. 2) and, hence, the number of pronounced low-frequency maxima in the power spectrum change on transiting from the flow separation to the flow reattachment regions.

Study of the spectrum P_r behind insertions of differing severity, but with the same length and at equal values of the flow Reynolds number shows that (Fig. 7):

(a) the shape of the spectrum is practically independent of S;
(b) the spectrum level generally increases/decreases as S increases/decreases;

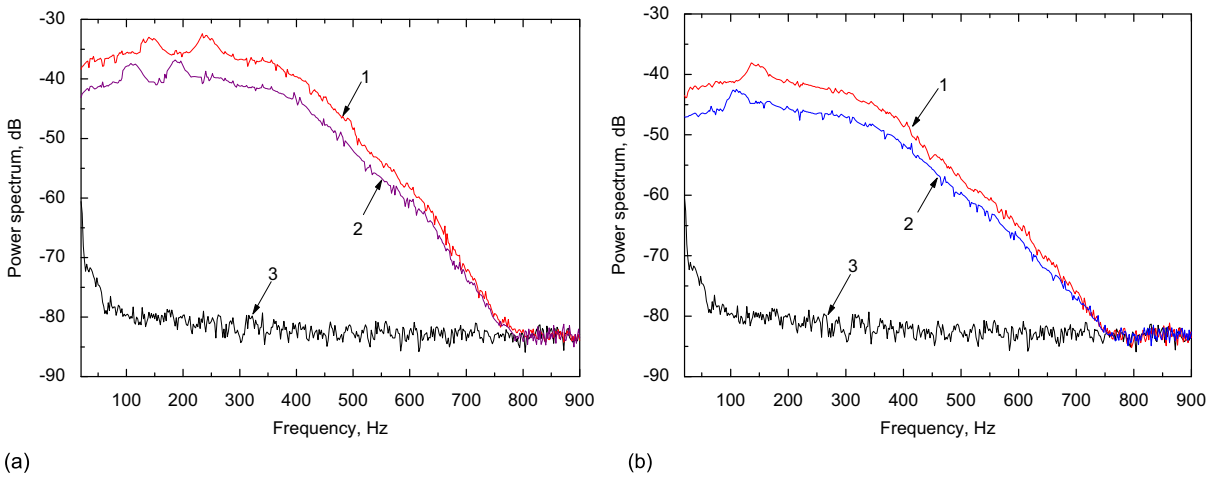

Fig. 8. Power spectrum of the wall pressure fluctuations in a rigid pipe, P_r, behind the narrowing ($d = 10$ mm, $S = 69.14\%$, $l = 20$ mm) at the points (a) $z = L^{(r)}_{\max}$ and (b) $z = 4D$: 1—$U = 0.35$ m/s {$\mathrm{Re}_D = 6300$); 2—$U = 0.27$ m/s ($\mathrm{Re}_D = 4860$}; 3—background noise.

(c) the locations of the pronounced low-frequency maxima in the spectrum change with S in accordance with changes in the frequencies (6)–(8).

The first observation arises because the general structure of the disturbed flow and the wall pressure fluctuation field behind a narrowing does not change significantly with S. The second effect is due to the corresponding increase/decrease in the flow and pressure field energy. The third feature is caused by changes in sizes and speeds of the large-scale eddies in the flow regions I and II, and, hence, the corresponding changes of their frequencies $f^{(1)}_{ch}$, ..., $f^{(3)}_{ch}$.

The influence of the flow Reynolds number on the spectrum P_r in the flow domains I and II is illustrated in Fig. 8, where the spectra generated by the same narrowing at different values of Re_D are shown. Comparative analysis of curves 1 and 2 for each flow domain shows that the variations in the spectrum P_r are qualitatively similar to those due to changes in S, namely:

(i) change of Re_D does not significantly affect the shape of the spectrum;
(ii) increase/decrease of Re_D results in a general increase/decrease in the spectrum level;
(iii) change in Re_D causes change of the locations of the pronounced low-frequency maxima in the spectrum P_r in accordance with changes of the frequencies (6)–(8).

The explanation of these effects is similar to that due to changes in S.

Finally, the effect of the narrowing length on the spectrum P_r is not as significant as that of S or Re_D. More specifically:

(i) the shape of the spectrum and the locations of its maxima near the frequencies $f^{(1)}_{ch}$, ..., $f^{(3)}_{ch}$ are practically insensitive to changes in l;
(ii) a significant (i.e., around 50%) increase/decrease in l about the value of 20 mm [9] (at approximately $S > 47\%$ and $\mathrm{Re}_D > 1150$ [9]) generally results in an insignificant (i.e., up to a few dB depending on z, f, S and(or) Re_D) decrease/increase in the spectrum level.

The insensitivity of the spectrum shape to changes in l can be explained by the corresponding invariance of the general structure of the flow and the wall pressure field behind a narrowing. Invariance of the locations of the pronounced low-frequency maxima in the function P_r is due to the invariance of sizes and speeds of the large-scale vortex formations in the flow regions I and II with changes in the narrowing length. The decrease/increase in the spectrum amplitude with an increase/decrease in l is caused by the corresponding increase/decrease of flow energy dissipation in the narrowing due to the increase/decrease of the viscous forces there.

3.2.2. Power spectrum of the wall pressure fluctuations in an elastic pipe

The wall pressure power spectrum for the flow regions I and II in an elastic pipe, P_e, (see curve 1 in Figs. 6(a) and (b)) looks, in general, like that in a rigid pipe. However, there are some differences in the low-frequency domain. Firstly, here the level of the elastic pipe spectrum is higher than that of the rigid pipe. For the glass-to-silicone pipe bending stiffness ratio and the flow velocity range chosen in this experiment this becomes noticeable (i.e., a relative difference between the spectral levels, $(10lgP_e - 10lgP_r)/10lgP_r \times 100\%$, of approximately 5–20% depending on measurement position, frequency, narrowing severity and Reynolds number) approximately for $S > 30\%$ and $\mathrm{Re}_d > 7000$. Secondly, some of the pronounced low-frequency maxima are shifted with respect to the rigid pipe case. More specifically, the first maximum of P_e in Fig. 6(a), and its maximum in Fig. 6(b), are located at somewhat lower frequencies than those of P_r. The location of the second spectral maximum in Fig. 6(a) remains practically constant. [Here it is valuable to compare the variations in the power spectrum with those in the pressure p_{rms} measured at the same location (see Section 3.1.2); it is observed that the spectrum P has more characteristic features indicating changes in the pipe wall properties than the pressure p_{rms} and these features in P are more sensitive to the noted changes than those in p_{rms}].

The aforementioned effects in the power spectrum arise due to the response of the flexible wall to the unsteady pressures (Blake, 1986; Borisyuk and Grinchenko, 1997; Crighton, 1983). More detailed explanation of the effects, including obtaining the quantitative relationships between the frequencies of the appropriate pronounced low-frequency maxima in the spectrum P_e and the parameters of the flow, pipe and narrowing, will require more detailed and sophisticated measurements.

Consideration of the variations in the spectrum P_e due to changes of the narrowing severity, S, length, l, and Reynolds number, Re_D, shows that generally they are similar to the corresponding variations in the spectrum P_r. Additionally, other conditions being equal, due to the response of the flexible wall to the unsteady pressures, the difference between the levels of the spectra P_e and P_r in the low-frequency domain increases/decreases with increasing/decreasing S and(or) Re_D.

3.3. Practical importance of the results

The results of this study can be practically applicable in developing non-invasive diagnostic techniques for vascular stenosis detection. For example, the pronounced low-frequency maxima in the wall pressure power spectrum downstream of the narrowing, found in this study, can also be detected in the power spectrum of both the wall pressure fluctuations after a vascular stenosis, P_t, and the acoustic field, P_{ac}, generated by a stenosed vessel (Borisyuk, 2002). The latter follows from the general relationship between P_t and P_{ac}; see Borisyuk (1998, 1999, 2002, 2003).

$$P_{ac} = T_b \times P_t, \tag{9}$$

where T_b is the transfer function which describes the processes of sound generation by the source P_t and sound transmission from the source to the body surface. The appearance of such maxima in the spectra P_t and P_{ac} associated with an originally healthy vessel would indicate a local reduction in the lumen area of vessel. Further increases (during the monitoring of the patient) in the spectrum levels and shifts (to higher frequencies) of some of the low-frequency peaks in the spectra P_t and[15] P_{ac} would imply progression in the stenosis severity. At this stage, the correlations between the frequencies of the low-frequency maxima and the experimental parameters (expressions (6)–(8)) can be used to find a first approximation to the stenosis diameter. The calculation proceeds as follows. Firstly, it is necessary to relate the frequencies of maxima in the spectrum P_{ac} (or P_t) to the characteristic frequencies identified in this work (i.e. $f_{ch}^{(1)}$, …, $f_{ch}^{(3)}$). Then, if the mean flow velocity U in the vessel under investigation is known, the stenosis diameter can be approximately determined either from (6) or (8), namely

$$d \propto \left(\frac{2UD^2}{f_{ch}^{(1)}}\right)^{1/3}, \quad d \propto \left(\frac{2UD}{f_{ch}^{(3)}}\right)^{1/2}.$$

If the velocity U is unknown, the diameter d can be found, for example, from the system of equations (6) and (8), namely

$$d \propto \frac{f_{ch}^{(3)}}{f_{ch}^{(1)}} D.$$

[15]From expression (9), any such behaviour in the spectrum P_t with S will be mirrored in P_{ac}.

Other pairings of Eqs. (6), (7) and (8) will give us additional approximate estimates for the stenosis diameter. The real value of d should be close to these estimates.

There can exist cases when the longitudinal dimension of a mild, but detectable, vessel narrowing grows with time, and the narrowing severity remains unchanged. This can lead to a decrease in the levels of the spectra P_t (as found in Section 3.2) and P_{ac} (see expression (9)), and hence to reduced differences with the corresponding recordings made when the vessel was healthy. Consequently, there can exist situations when, on reaching some critical value of stenosis length, $l = l_{cr}$, the difference between noise levels from the healthy and diseased vessels becomes so small that a previously detectable stenosis becomes practically undetectable by basic acoustic diagnosis techniques. The only remaining signs of a stenosis may now be the low-frequency spectral maxima near the frequencies (6)–(8), if distinguishable. If even these maxima cannot be observed, a vascular narrowing cannot then be detected. These considerations suggest that researchers should attempt to establish the quantitative relationship between l_{cr} and the parameters of the flow, vessel and stenosis.

The increase in level of the spectrum P_t, and hence also of the spectrum P_{ac}, due to an increase in the flow Reynolds number (see Section 3.2 and expression (9)) suggests that it may be easier to detect stenoses under elevated flow conditions (manual labour) rather than under normal flow conditions (patient at rest).

In the study of stenosis hydrodynamics, the concept of a 'critical' stenosis is used, with the critical stenosis, S_{cr}, usually interpreted as one for which a small (just a few percent) further reduction in lumen area will cause significant (more than 10%) changes in the characteristics of the hydrodynamic field. Typically (Mirolyubov, 1983; Young, 1979), it is found that the values for S_{cr} vary widely (50–90%) depending on the patient. In this series of experiments [see also Borisyuk (2002)], it was possible to detect milder narrowings for which $S \approx 20\%$. This may be a reason for introducing the 'critical' stenosis into the study of acoustic diagnosis techniques, and might therefore stimulate researchers into finding the quantitative relationships between S_{cr} and the parameters of the stenosis, vessel and flow.

4. Conclusions

An investigation methodology has been developed, and an experimental facility created, in order to model the wall pressure fluctuations in a larger blood vessel immediately behind a stenosis. The assumptions made in modelling the blood, flow, vessel and stenosis conform with those generally accepted in this area of research. One can therefore say that the characteristics of the wall pressure fluctuations obtained in this experiment are, to a first order of approximation, similar to those which exist in reality. Analysis of these experimental characteristics, carried out for typical values of flow, vessel and narrowing parameters, permits the following conclusions to be drawn.

1. A local pipe narrowing disturbs the flow, resulting in a sharp increase of the wall pressure fluctuations in a finite region immediately behind the narrowing. In this region, the rms wall pressure, p_{rms}, reaches a maximum at a location that is always before the flow reattachment point.
2. The length of the most disturbed and the total disturbed flow regions behind the narrowing for rigid and elastic pipes does not exceed $7D$ and $12D$, respectively.[16]
3. For the narrowing shape chosen, the distance $L_{\max}$ from the narrowing to the point of maximum pressure p_{rms} lies approximately in the range 1.3–2.6 D for both pipes. This distance increases/decreases as the jet Reynolds number, Re_d, and(or) the narrowing severity, S, increases/decreases in accordance with estimates (2a, b) and (4).[16]
4. For $\mathrm{Re}_d > 8500$ in a rigid pipe and $\mathrm{Re}_d > 9000$ in an elastic pipe, the maximum pressure $(p_{\mathrm{rms}})_{\max}$ at the point $z = L_{\max}$ is approximately proportional to the jet dynamic pressure behind the narrowing, $0.5\rho u^2$, and the ratio of the diameters of the narrowed and normal segments of the pipe, d/D (see estimates (3) and (5)[16]).
5. For the pipes chosen and the velocity range used in this study, a decrease in the pipe wall bending stiffness generally results in an increase in the rms wall pressure. However, this increase only becomes noticeable (i.e., approximately 5–13% of the rigid-pipe value depending on measurement position, narrowing severity and Reynolds number) approximately for $S \geq 75\%$ and $\mathrm{Re}_d \geq 9000$.
6. In general, the rms wall pressure behind the narrowing in rigid, $p^{(r)}_{\mathrm{rms}}$, and elastic, $p^{(e)}_{\mathrm{rms}}$, pipes, as well as the difference $\Delta p_{\mathrm{rms}} = p^{(e)}_{\mathrm{rms}} - p^{(r)}_{\mathrm{rms}}$ increases/decreases as the narrowing severity, S, and(or) the flow Reynolds number, Re_D, increases/decreases. The pressures $p^{(r)}_{\mathrm{rms}}$ and $p^{(e)}_{\mathrm{rms}}$ weakly decrease/increase with an increase/decrease of the narrowing length, l.

[16]These estimates will be shown in a future paper to be generally valid for the smoother and more streamlined narrowing shapes, axisymmetric and non-axisymmetric, which were also used in this series of experiments. From this, it can be concluded that these estimates are more universal than corresponding estimates currently available in the scientific literature.

7. The wall pressure power spectrum in the most disturbed flow region behind a narrowing in a rigid pipe, P_r, generally looks like that of the wall pressure fluctuations in a fully-developed turbulent flow in a rigid pipe without narrowing. A characteristic feature of the spectrum P_r is that it has local pronounced low-frequency maxima. These maxima are associated with large-scale vortex structures in the flow separation and reattachment regions, and their frequencies match the characteristic frequencies of these vortex structures (see expressions (6)–(8)).
8. The power spectrum of the wall pressure fluctuations in the most disturbed flow region in an elastic pipe, P_e, is generally similar to P_r. The differences between P_e and P_r are as follows. Firstly, in the low-frequency domain, the level of the spectrum P_e is higher than that of P_r [however, for the pipes and the velocity range used in this study, the difference only reaches the 5 – 20% range (depending on measurement position, frequency, narrowing severity and Reynolds number) approximately for $S>30\%$ and $\mathrm{Re}_d>7000$]. Secondly, some of the pronounced low-frequency maxima of the spectrum P_e are shifted with respect to the corresponding maxima in the spectrum P_r.
9. The shape of the spectra P_r and P_e does not change significantly with S and(or) Re_D; their levels and the differences between them generally increase/decrease as S and(or) Re_D increases/decreases, and the locations of their low-frequency maxima change with changes in these parameters (in case of P_r the changes in the locations of the maxima are in accordance with (6)–(8); as for the appropriate maxima in P_e, more detailed and sophisticated measurements are required to relate their locations to the parameters of the flow, vessel and narrowing). An increase/decrease of the narrowing length causes a weak decrease/increase in the levels of the spectra.
10. The overall level and the number of low-frequency maxima in the spectra P_r and P_e decrease as the distance from the narrowing increases (i.e. when transiting from the flow separation to flow reattachment regions).
11. The wall pressure power spectrum, P, has more characteristic features indicating changes in the pipe wall properties than the rms wall pressure, p_{rms}, and these features in P are more sensitive to the noted changes than those in p_{rms}.

Acknowledgements

The author gratefully acknowledges the financial support of the Alexander von Humboldt Foundation (Germany).

References

Abdallah, S.A., Hwang, N.H.C., 1988. Arterial stenosis murmurs: an analysis of flow and pressure fields. Journal of the Acoustical Society of America 83, 318–334.

Berger, S.A., Jou, L.D., 2000. Flows in stenotic vessels. Annual Review of Fluid Mechanics 32, 347–382.

Blake, W.K., 1986. Mechanics of Flow-Induced Sound and Vibration, vols. 1 and 2. Academic Press, New York.

Bluestein, D., Einav, S., 1995. The effect of varying degrees of stenosis on the characteristics of turbulent pulsatile flow through heart valves. Journal of Biomechanics 28 (8), 915–924.

Borisyuk, A.O., Grinchenko, V.T., 1997. Vibration and noise generation by elastic elements excited by a turbulent flow. Journal of Sound and Vibration 204, 213–237.

Borisyuk, A.O., 1998. Modeling of the acoustic properties of a larger human blood vessel. Acoustic Bulletin 1 (3), 3–13.

Borisyuk, A.O., 1999. Noise field in the human chest due to turbulent flow in a larger blood vessel. Flow, Turbulence and Combustion 61, 269–284.

Borisyuk, A.O., 2002. Experimental study of noise produced by steady flow through a simulated vascular stenosis. Journal of Sound and Vibration 256, 475–498.

Borisyuk, A.O., 2003. Model study of noise field in the human chest due to turbulent flow in a larger blood vessel. Journal of Fluids and Structures 17, 1095–1110.

Clark, C., 1977. Turbulent wall pressure measurements in a model of aortic stenosis. Journal of Biomechanics 10, 461–472.

Crighton, D.G., 1983. Long range acoustic scattering by surface inhomogeneities beneath a turbulent boundary layer. In: Proceedings of the International Symposium on Turbulence-Induced Vibrations and Noise of Structures, Boston, pp. 107–123.

Duncan, G.W., Gruber, J.O., Dewey Jr., C.F., Myers, G.S., Lees, R.S., 1975. Evaluation of carotid stenosis by phonoangiography. New England Journal of Medicine 293, 1124–1128.

Fredberg, J.J., 1977. Origin and character of vascular murmurs: model studies. Journal of the Acoustical Society of America 61, 1077–1085.

Giddens, D.P., Mabon, R.F., Cassanova, R.A., 1976. Measurements of disordered flow distal to subtotal vascular stenosis in the thoracic aorta of canines. Circulation Research 39, 112–119.

Iudicello, F., Collins, M.W., Henry, F.S., Javris, J.C., Shortland, A., Black, R., Salmons, S., 1997. A review of modelling for arterial vessels-simplified ventricular geometries. In: Advances in Fluid Mechanics. Computational Mechanics Publications, Southampton, Boston, pp. 179–194.

Kim, B., Corcoran, W.K., 1974. Experimental measurement of turbulence spectra distal to stenosis. Journal of Biomechanics 7, 335–342.

Kirkeeide, R.L., Young, D.F., Cholvin, N.R., 1977. Wall vibrations induced by flow through simulated stenoses in models and arteries. Journal of Biomechanics 10, 431–441.

Lees, R.S., Dewey Jr., C.F., 1970. Phonoangiography: a new noninvasive diagnostic method for studying arterial disease. Proceedings of the National Academy of Sciences 67, 935–942.

Mirolyubov, S.G., 1983. Hydrodynamics of stenosis. Modern Problems in Biomechanics 1, 73–136 (in Russian).

Pedrizzetti, G., 1996. Unsteady tube flow over an expansion. Journal of Fluid Mechanics 310, 89–111.

Pitts, W.H., Dewey Jr., C.F., 1979. Spectral and temporal characteristics of post-stenotic turbulent wall pressure fluctuations. ASME Journal of Biomechanical Engineering 101, 89–95.

Tobin, R.J., Chang, I.D., 1976. Wall pressure spectra scaling downstream of stenoses in steady tube flow. Journal of Biomechanics 9, 633–640.

Voskoboinik, V.A., Grinchenko, V.T., Makarenkov, A.P., 2000. Convection speeds of the coherent vortex structures in turbulent boundary layer on a cylinder. Acoustic Bulletin 3, 21–29 (in Russian).

Voskoboinik, V.A., Grinchenko, V.T., Makarenkov, A.P., 2002. Pseudo-sound behind an obstacle on a cylinder in axial flow. Acoustic Bulletin 5, 22–36 (in Russian).

Wang, J., Tie, B., Welkowitz, W., Semmlow, J.L., Kostis, J.B., 1990. Modeling sound generation in stenosed coronary arteries. IEEE Transactions of Biomedical Engineering 37, 1087–1094.

Young, D.F., 1979. Fluid mechanics of arterial stenoses. Journal of Biomechanical Engineering 101, 157–175.